NeuroImage 257 (2022) 119320

Contents lists available at ScienceDirect

NeuroImage

journal homepage: www.elsevier.com/locate/neuroimage

Functional connectivity maps of theta/alpha and beta coherence within the subthalamic nucleus region

Bernadette C.M. van Wijk[a,b,c,d,*], Wolf-Julian Neumann[c], Daniel Kroneberg[c], Andreas Horn[c,f,g], Friederike Irmen[c], Tilmann H. Sander[e], Qiang Wang[c], Vladimir Litvak[d], Andrea A. Kühn[c,h,i]

[a] Department of Human Movement Sciences, Faculty of Behavioural and Movement Sciences, Vrije Universiteit Amsterdam, the Netherlands
[b] Integrative Model-based Cognitive Neuroscience Research Unit, Department of Psychology, University of Amsterdam, the Netherlands
[c] Movement Disorder and Neuromodulation Unit, Department of Neurology, Charité – Universitätsmedizin Berlin, corporate member of Freie Universität Berlin, Humboldt-Universität zu Berlin, and Berlin Institute of Health, Berlin, Germany
[d] Wellcome Centre for Human Neuroimaging, University College London, UK
[e] Physikalisch-Technische Bundesanstalt, Institut Berlin, Germany
[f] Center for Brain Circuit Therapeutics, Department of Neurology, Brigham & Women's Hospital, Harvard Medical School, Boston, USA
[g] MGH Neurosurgery & Center for Neurotechnology and Neurorecovery (CNTR), MGH Neurology, Massachusetts General Hospital, Harvard Medical School, Boston, USA
[h] NeuroCure Clinical Research Centre, Charité – Universitätsmedizin Berlin, Germany
[i] DZNE, German Center for Degenerative Diseases, Berlin, Germany

ARTICLE INFO

Keywords:
Subthalamic nucleus
Functional connectivity
Parkinson's disease
Deep brain stimulation
Magnetoencephalography

ABSTRACT

The subthalamic nucleus (STN) is a primary target for deep brain stimulation in Parkinson's disease (PD). Although small in size, the STN is commonly partitioned into sensorimotor, cognitive/associative, and limbic subregions based on its structural connectivity profile to cortical areas. We investigated whether such a regional specialization is also supported by functional connectivity between local field potential recordings and simultaneous magnetoencephalography. Using a novel data set of 21 PD patients, we replicated previously reported cortico-STN coherence networks in the theta/alpha and beta frequency ranges, and looked for the spatial distribution of these networks within the STN region. Although theta/alpha and beta coherence peaks were both observed in on-medication recordings from electrode contacts at several locations within and around the STN, sites with theta/alpha coherence peaks were situated at significantly more inferior MNI coordinates than beta coherence peaks. Sites with only theta/alpha coherence peaks, i.e. without distinct beta coherence, were mostly located near the border of sensorimotor and cognitive/associative subregions as defined by a tractography-based atlas of the STN. Peak coherence values were largely unaltered by the medication state of the subject, however, theta/alpha peaks were more often identified in recordings obtained after administration of dopaminergic medication. Our findings suggest the existence of a frequency-specific topography of cortico-STN coherence within the STN, albeit with considerable spatial overlap between functional networks. Consequently, optimization of deep brain stimulation targeting might remain a trade-off between alleviating motor symptoms and avoiding adverse neuropsychiatric side effects.

1. Introduction

The clinical success of deep brain stimulation (DBS) treatment for advanced Parkinson's disease has stirred the interest in the anatomical and functional organisation of the subthalamic nucleus (STN) across research labs worldwide. As the smallest nucleus of the basal ganglia, the STN predominantly receives input from the external pallidum, thalamus, and several brain stem nuclei (Parent and Hazrati, 1995) in addition to input from direct cortical projections (Nambu et al., 2002). Anterograde tracing work in animals (Haynes and Haber, 2013; Parent and Hazrati, 1995) and diffusion-weighted imaging studies in humans (Accolla et al., 2014; Ewert et al., 2018; Lambert et al., 2012) have revealed a topographic organisation of these structural connections that has motivated a partitioning of the STN into sensorimotor, cognitive/associative, and limbic subregions. Although such a tripartite subdivision forms an attractive hypothesis for the relation between the exact anatomical coordinates of implanted DBS electrodes and the observed effect of stimulation on motor and neuropsychiatric symptoms (Temel et al., 2005), it has also been met with scepticism due to in-

* Corresponding author at: Department of Human Movement Sciences, Faculty of Behavioural and Movement Sciences, Vrije Universiteit Amsterdam, the Netherlands.
E-mail address: b.c.m.van.wijk@vu.nl (B.C.M. van Wijk).

https://doi.org/10.1016/j.neuroimage.2022.119320.
Received 12 November 2021; Received in revised form 10 May 2022; Accepted 12 May 2022
Available online 14 May 2022.

consistent findings across studies regarding the number and location of subregions (Keuken et al., 2012) and the large degree of overlap in terminal fields from cortical projections (Alkemade et al., 2015).

Local field potential (LFP) recordings from DBS electrodes in combination with simultaneous magnetoencephalography (MEG) or electroencephalography (EEG) allow for investigating functional connectivity between the STN and cortical regions. This has revealed a number of frequency-specific and spatially distinct networks that have proven replicable across patient cohorts from different medical centres. In rest recordings, alpha band coherence (~7–12 Hz) has been detected with superior temporal gyrus and brainstem, whereas beta band coherence (~13–35 Hz) localizes to (pre-)motor cortex (Hirschmann et al., 2011; Litvak et al., 2011a). A further distinction can be made between coherence in the low-beta frequency range (~13–21 Hz) with lateral, and high-beta coherence (~21–35 Hz) with mesial (pre-)motor areas (Oswal et al., 2016; Toledo et al., 2014). Less replicable have been the investigations into modulations of cortico-STN coherence by dopaminergic medication and the relation between coherence values and Parkinsonian symptom severity (Hirschmann et al., 2013; Litvak et al., 2012; Oswal et al., 2013a), therefore leaving unresolved to what extent these networks are disease-dependent.

Despite the clearly distinct cortical topography of alpha and beta band cortico-STN coherence, it remains unknown whether these separate networks can also be associated with distinct locations within the STN as a signature of regional specialization. We address this question in the current study by reporting results from a new dataset of simultaneous LFP and MEG recordings obtained from patients with Parkinson's disease who are undergoing STN-DBS treatment. We utilised the interindividual variability in electrode positions within and around the STN that is inherent to the surgical procedure, in order to map the locations with theta/alpha and/or beta coherence peaks. In addition, we examined the effect of dopaminergic state on the occurrence of cortico-STN coherence. Despite the limited spatial resolution of macroelectrode recordings, we were able to show that recording sites with only theta/alpha coherence peaks were located significantly inferior to sites with only beta coherence. Our findings point at regional specialization within the STN region, albeit with considerable spatial overlap between functional networks.

2. Methods

2.1. Patients and data acquisition

Simultaneous whole-head MEG and LFP recordings from DBS electrodes have been collected by our centre over several years. We included recordings from our database from 21 patients who underwent bilateral implantation of DBS macroelectrodes in STN with Medtronic model 3389 (Minneapolis, MN, USA) for treatment of Parkinson's disease, and for whom both pre-operative and post-operative structural imaging were available. These data were acquired over a time period of 4.5 years. We considered recordings that were acquired while patients were either on their regular dose of dopaminergic medication (ON) or after 12 h withdrawal (OFF). Thirteen patients participated in both OFF and ON conditions that were collected in consecutive sessions before (OFF) and 30 min after administration of a fast-acting dopaminergic agent (Madopar LT, ON). Seven patients participated in the ON condition only, and one patient in the OFF condition only. All patients (14 male, 7 female) underwent surgery at the Charité – Universitätsmedizin Berlin 1–7 days prior to the recordings. Mean age at the time of recordings was 60 years (range 39–72) and the average disease duration 10 years (range 3–25). For 15 patients we had UPDRS assessments available that were taken around the day of the recording session. Their total UPDRS-III scores were on average 20.4 (range 5–48) ON medication and 31.5 (range 7–70) OFF medication. The remaining patients were assessed preoperatively. Their total UPDRS-III scores were on average 24.1 (range 16–41) ON medication and 42.3 (range 24–71) OFF medication.

On the day of the experiment, the subject was transferred from the hospital ward to the nearby Physikalisch Technische Bundesanstalt, where we used the 125-channel MEG system (ET 160, Yokogawa Electric. Corp., Tokyo, Japan). LFP recordings were obtained simultaneously with MEG by connecting the externalized extensions from the DBS leads to an EEG amplifier. A 150 Hz low-pass filter and sampling rate of 1000 Hz was used for the first 3 subjects, and a 400 Hz low-pass filter and sampling rate of 2000 Hz for all subsequent subjects. For each subject, 3-4 min eyes-open rest recordings were acquired after which the session typically continued with another experimental task. Here, we only consider the rest recordings. In addition, we made use of preoperative MRI (T1- and T2-weighted, 3T, all patients) and post-operative MRI (T2-weighted, 1.5T, 12 patients) or CT (9 patients) scans that were acquired as part of the clinical routine.

The study was approved by the local ethics committee of the Charité – Universitätsmedizin Berlin, Campus Virchow Klinikum, and was conducted in accordance with the declaration of Helsinki. Patients were informed orally and in writing of the experimental procedures and were all given at least 24 h to consider their participation. Informed consent forms were signed prior to the recordings.

2.2. Electrode localization

Surgical implantation of DBS electrodes was performed bilaterally and targeted at the dorsolateral part of the STN at the level of the anterior border of the red nucleus (at its maximum diameter). Electrode placement was guided by intraoperative microelectrode recordings and the patient's clinical response to stimulation. The neurosurgical team targets the lower border of the subthalamic nucleus as visualized in the preoperative MRI. During intraoperative microelectrode monitoring the ventral border is identified based on the neural firing pattern. Then, the centre of the lowermost contact is placed to coincide with the neurophysiologically identified ventral border. The placement of electrodes within STN and/or its direct vicinity was verified by postoperative MRI or CT for each patient. We used the inter-individual variability in electrode positions, which inherently arises from the surgical procedure and trajectory, to relate the presence of cortical-STN functional connectivity to anatomical location.

The Lead-DBS toolbox was used to enable group-level analyses in MNI space (Horn and Kühn, 2015) using the default work-flow of version 2.1.7 as described in Horn et al. (2019). This involved the localization of implanted DBS electrodes based on the postoperative CT or MRI scan, linear co-registration with the pre-operative scans, and non-linear warping to the ICBM152 nonlinear asymmetric 2009b ("MNI") template (Fonov et al., 2011) using the SyN registration approach as implemented in Advanced Normalization Tools (ANTs) (Avants et al., 2008). 3D electrode trajectories were automatically detected from the hypointensities/hyperdensities caused by the electrode leads on the postoperative scans, and were subsequently refined manually to match the positioning of the electrode contacts. Results of each processing step were carefully inspected visually and re-run until no further improvement was obtained. The electrode model used to obtain LFP recordings, Medtronic 3389, contains four contact points with a diameter of 1.27 mm, length of 1.5 mm and an inter-contact spacing of 0.5 mm (i.e., 2 mm from contact center to contact center). The Euclidean midpoint between two adjacent contacts was taken as the location of the corresponding bipolar recording. The MNI locations for the left hemisphere were projected towards the right hemisphere via non-linear registration to the mirrored template scan. The DISTAL atlas (Ewert et al., 2018) was used to visualize results with respect to sensorimotor, cognitive/associative, and limbic subregions that were informed by cortical-STN structural connectivity.

2.3. Cortico-STN coherence

As a first step, we verified whether we could identify the cortico-STN networks at distinct frequencies and cortical origins that were reported

in earlier studies (Hirschmann et al., 2011; Litvak et al., 2011a). We also investigated how cortico-STN coherence was altered by the administration of dopaminergic medication in order to test whether the medication state of the patient could affect the localization of coherence networks within the STN. Our analyses were performed by making use of SPM12 (Litvak et al., 2011b) and FieldTrip (as embedded in SPM12; Oostenveld et al., 2011) Matlab toolboxes.

Prior to the coherence analysis, bipolar derivations were taken between adjacent DBS electrode contacts, yielding three LFP time series per hemisphere. Both MEG and LFP time series were high-pass filtered with cut-off frequency 1 Hz and notch-filtered with ±2 Hz to remove the 50 Hz component and its higher-order harmonics. The continuous time series were then divided into epochs of 3 s (first 3 subjects) or 3.5 s (remaining subjects). Epochs during which the amplitude of the LFP channels exceeded 0.3 mV were removed from subsequent analysis together with one of the MEG channels that was consistently noisy across recording sessions.

On the sensor level, we computed coherence between the time series of each STN contact pair and all MEG sensors for frequencies between 2 and 100 Hz with 0.25 Hz steps and 2 Hz smoothing using the Slepian sequence multitaper method as implemented in FieldTrip (Thomson, 1982). The resulting coherence spectra were then averaged across the three contact pairs per hemisphere and all MEG sensors in order to obtain a single overall coherence spectrum per subject, hemisphere, and condition. This step served to determine the frequency ranges of interest for possibly distinct cortico-STN networks, to select individual coherence peak frequencies (see below), and to test for frequency-specific (but spatially global) effects of medication. Given the unbalanced experimental design of our study, we performed our statistical assessment with a linear mixed-effects analysis (using Matlab's *fitlme* function, R2019a, The Mathworks Inc., Natick, USA) with the factors *Condition* (ON *vs.* OFF) and *Hemisphere* (left *vs.* right) as fixed effects, and a factor *Subject* as random effect. This was repeated for the average coherence within 2 Hz frequency bands across the spectrum. In addition, we visualized coherence values averaged across contact pairs, subjects, and within selected frequency ranges as a scalp topography. Together, these steps led to the identification of two separate functional networks with coherence peaks in a low-frequency range (theta/alpha, 4–13 Hz) and in the beta band (13–35 Hz).

In order to increase the sensitivity of our subsequent source localization analysis, we marked the frequencies of coherence peaks in both bands in individual spectra that were averaged across contact pairs per hemisphere and all MEG sensors. We combined the theta and alpha frequency ranges into a single 'theta/alpha' band as coherence peak frequencies often occurred around the boundary between the conventionally used definition of these bands. We localized the cortical sources for cortico-STN coherence within the range of ±2.5 Hz around the selected theta/alpha peaks and within ±5 Hz around the selected beta peaks with the dynamic imaging of coherent sources (DICS) beamforming method (Gross et al., 2001). The T1-weighted MRI scan from each subject was warped to MNI space and co-registered to the MEG recordings via the positions of the nasion and pre-auricular fiducials. Potential source locations were defined as a 3D grid in MNI space with 5 mm spacing within a volume bounded by the inner surface of the skull. The inverse-normalized canonical mesh of the inner skull was used to construct the forward model based on the subject's individual anatomy (Mattout et al., 2007) with the lead field for each (inverse-normalized) grid point computed via a single-shell head model (Nolte, 2003). Again, the multitaper method was used for computing the cross-spectral density and the final images of source level cortico-STN coherence values. No further (global) normalization of these images was applied.

Images for the left STN were reflected with respect to the sagittal plane to make them directly comparable with those for the right STN and to allow interpretation of findings in terms of ipsilateral and contralateral hemisphere. We then implemented a linear mixed-effects analysis using SPM's flexible factorial design. Again, the factors *Condition* (ON *vs.* OFF) and *Hemisphere* (left *vs.* right) were set as fixed effects, and a factor *Subject* as random effect. Furthermore, we assessed which cortical regions showed significantly higher coherence than expected by chance through the comparison with coherence values obtained after shuffling the order of epochs for the LFP data (cf. Neumann et al., 2015). One such image was generated for each available regular image per subject. A factor *Shuffled* (regular *vs.* shuffled) was added to the design and we tested for its main effect. In addition, we included the *Condition*Shuffled* and *Hemisphere*Shuffled* interaction terms. All results were assessed at peak-level with α=.001 to reduce the risk of false positives due to the large number of voxel-wise comparisons.

2.4. Regional specialization within STN

Our main objective was to identify the location of theta/alpha and beta cortico-STN coherence within the subthalamic nucleus region. A clear spatial separation of theta/alpha and beta coherence source origins would suggest the STN to have functionally specialized regions, based on the prevailing notion that neural oscillations in distinct frequency bands serve distinct functional roles. Sensor-level STN-coherence spectra averaged across all MEG sensors were used for this analysis in order to avoid arbitrary selection of cortical source locations for some of the recordings. We carefully inspected these coherence spectra for each contact pair individually and classified them into one of four categories: (i) coherence peak in the theta/alpha range only; (ii) coherence peak in the beta range only; (iii) coherence peaks in both theta/alpha and beta ranges, or (iv) no distinct coherence peaks discernible. To determine whether significant coherence peaks were present, we obtained 100 surrogate spectra after randomly shuffling the order of epochs for the STN data. We adopted a conservative approach and only labelled extrema as peaks if their amplitude exceeded that of at least 99 surrogate spectra for all points within a minimum frequency range of 3 Hz around theta/alpha peaks and 5 Hz around beta peaks. Additionally, extrema that could be attributed to the 1/f-like shape that was found to occur over lower frequencies for some recordings were not considered. The classification of peaks based on these criteria was visually inspected and corrected if deemed necessary.

The classification of individual contact pairs based on coherence peaks was combined with the corresponding electrode localizations obtained within Lead-DBS. This yielded the MNI-coordinates of each contact pair (through its Euclidean midpoint) within each category. These locations were statistically compared between categories in two ways. Firstly, we performed independent samples *t*-tests for the *x, y*, and *z*-coordinates separately. Secondly, we acknowledged that the STN is not fully spatially aligned with the MNI coordinate system and therefore projected the identified electrode locations on the 3 principal axes of the STN that were extracted from its Distal atlas image. The independent samples *t*-tests between categories were repeated for each of the three principal axes. Finally, we tested whether the locations within each category were more spatially clustered than expected by chance. For this, we computed the average Euclidean distance between the locations within each category and their centre point. This value was compared against a distribution of surrogate average Euclidean distances obtained from 10.000 iterations with shuffled category labels. Analyses were performed for ON and OFF medication conditions separately. All results were assessed at α = .05.

3. Results

3.1. Sensor-level cortico-STN coherence

The grand-averaged coherence spectrum revealed a clear peak in the beta frequency range (Fig. 1A) that was also visible in the individual spectra (Fig. 1B). A clear coherence peak in the theta/alpha frequency range could not be discerned in the grand-average but was present in the individual spectra. Overall, coherence appeared somewhat more

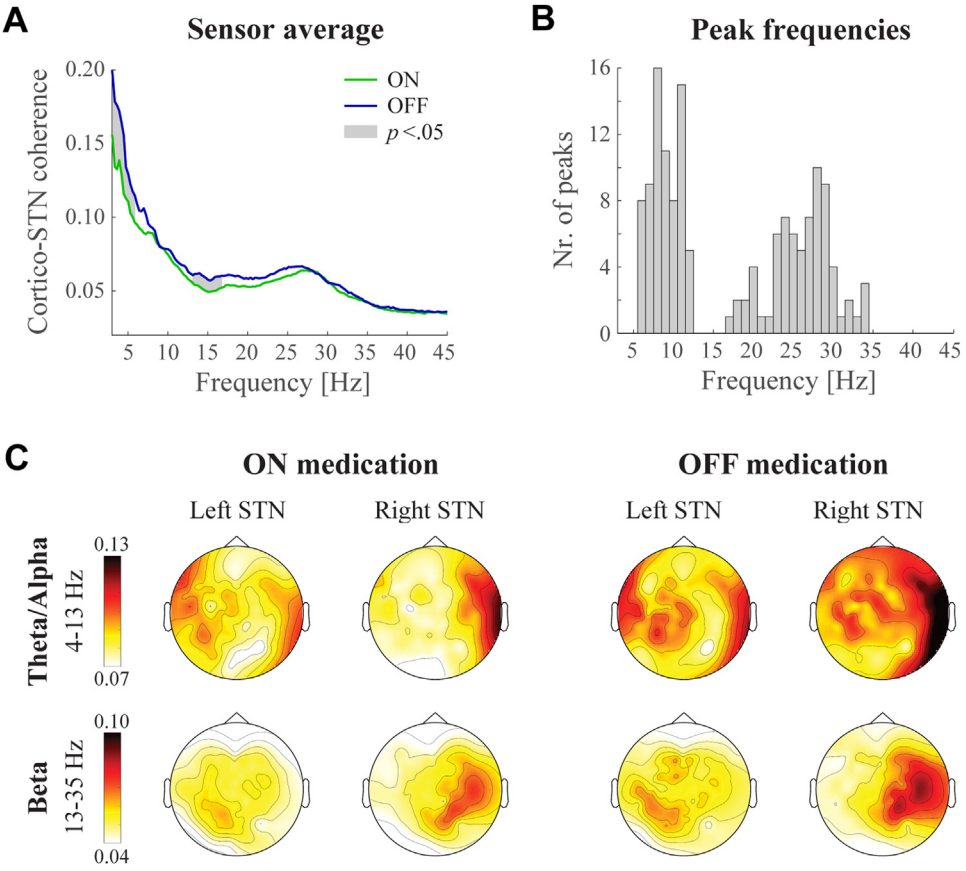

Fig. 1. Sensor-level cortico-STN coherence. (A) Coherence spectra averaged across all combinations of STN contact pairs and MEG sensors, and subjects. Average coherence values within 2 Hz frequency bins were statistically compared at group-level using a linear mixed-effects model. Bins with a significant main effect of *Condition* are indicated in grey. (B) Histogram of coherence peak frequencies selected for source localization. One theta/alpha (within 4–13 Hz) and one beta (within 13–35 Hz) peak was selected per hemisphere and medication condition for each subject. (C) Scalp topographies by hemisphere and medication condition. Coherence values were averaged across frequencies in the full theta/alpha and beta ranges, the three contact pairs per hemisphere, and all subjects from whom recordings were available. Topographies for coherence values only averaged around the individual peak coherence frequencies appear highly similar (not shown).

strongly for recordings obtained when subjects were withdrawn from medication compared to ON medication. Significant differences between medication states were found for frequencies at the lower end of the theta/alpha and beta frequency ranges. By contrast, coherence peaks in individual spectra were primarily detected for higher frequencies within these ranges. No significant main effect of *Condition* was found when repeating the statistical analysis with average coherence values within ±2.5 Hz around the individual theta/alpha coherence peak frequencies ($F(1,65)=0.36$, $p = .549$), or within ±5 Hz around the individual beta coherence peak frequencies ($F(1,65) = 0.45$, $p = .503$).

In later analyses, we used the average sensor-level coherence to localize cortico-STN coherence within the STN region. In Fig. 1C we visualize the grand-average scalp topographies to get an impression of which sensors contribute most to the average. The topographies revealed coherence to be largely lateralized to MEG sensors overlying the ipsilateral hemisphere. They were also found to be frequency band-dependent, with strongest theta/alpha coherence for the most lateral sensors and beta coherence for more central sensors hinting at distinct underlying cortical sources. Although the scalp topographies suggest that coherence for the right STN was stronger compared to the left STN, no significant main effect of *Hemisphere* was found for any of the frequency bins in the sensor-averaged coherence spectrum. Topographies for the average and difference between ON and OFF medication conditions are shown in Supplementary Fig. 1.

3.2. Source-level cortico-STN coherence

DICS source localisation was performed to verify the cortical source locations of theta/alpha and beta cortico-STN coherence. Significant sources were identified with a linear mixed-effects analysis by comparing regular coherence images against coherence images obtained after shuffling the order of epochs for STN data. Results are displayed in Fig. 2. For the theta/alpha band, the main effect of *Shuffled* revealed significant sources in central locations of the brain with the thalamus as location with the highest *F*-value (peak at [-2 -22 2] mm: $F(1,108) = 50.86$, $p < .001$. A cortical source in the Rolandic operculum became apparent in the *Hemisphere*Shuffled* interaction (peak at [36 -20 20] mm: $F(1,108) = 13.76$, $p < .001$), reflecting stronger coherence values for the right compared to the left STN. The grand-averaged coherence images (top row of Fig. 2) show this source even more clearly. For the beta band, a large cluster was found with its peak location near pre-motor cortex (peak at [46 6 56] mm: $F(1,96)=47.09$, $p < .001$). The peak location of grand-averaged coherence was found to be located more mesial compared to the statistical result, and is in line with the location for which high-beta coherence was previously reported (Oswal et al., 2016; Toledo et al., 2014). Our identified cortical sources of theta/alpha and beta coherence show a strong resemblance with previous reports of cortico-STN alpha coherence with sources in superior temporal gyrus and brainstem and beta coherence with sources in (pre-)motor cortex (Hirschmann et al., 2011; Litvak et al., 2011a), hence providing a replication of spatially and spectrally distinct cortico-STN networks in an independent data set.

The only significant main effect of *Condition* was observed for a small cluster in visual cortex for theta/alpha coherence (peak value at [4 -96 6] mm: $F(1,45) = 19.11$, $p < .001$). No significant sources for the main effect of *Hemisphere* were found for either theta/alpha or beta coherence at $\alpha<.001$. The source level analysis may have been less sensitive to the main effects of *Condition* found at the sensor-level as the frequency ranges were dissimilar. Nevertheless, we focused our source analysis on the coherence peak frequencies as a more robust marker of the functional connectivity networks that we aimed to identify. Results were similar with a less stringent α-level of .01.

3.3. Localization of cortico-STN coherence within STN

The final and main part of our analysis concerned the localization of theta/alpha and beta coherence within the subthalamic nucleus region. To this aim, we categorized the recordings from all STN contact

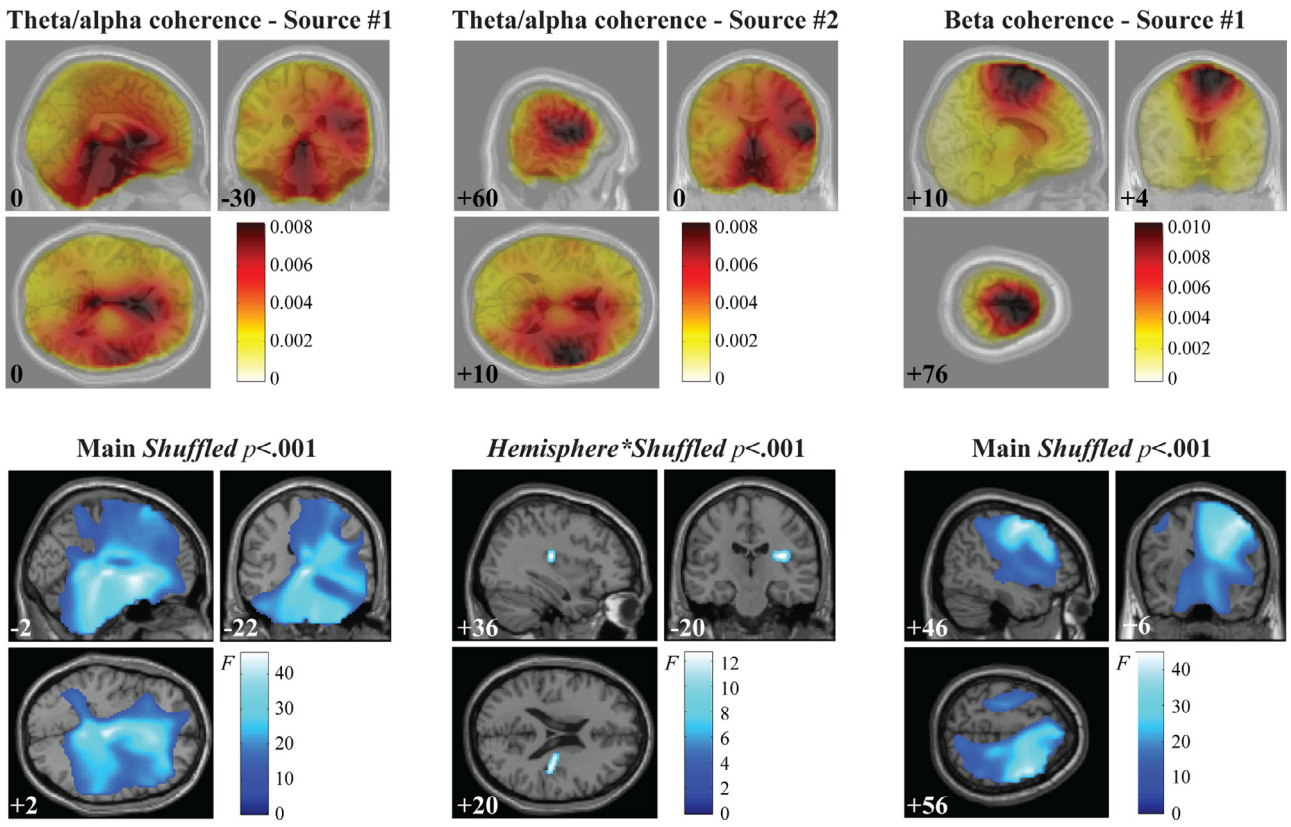

Fig. 2. Source-level cortico-STN coherence. The top row displays grand-averaged coherence values indicating at which locations coherence was largest at group-level. Peak locations for which coherence was found significantly higher compared to that obtained after shuffling the order of epochs are shown in the bottom row. These effects match the frequency band and source location in the top row. MNI coordinates of the displayed slices are indicated in the bottom left corner of each panel and correspond to the location at which peak values were found. Shown images were smoothed with a 4 mm isotropic Gaussian kernel for visualization purposes.

Table 1
Number of STN contact pairs selected within each coherence category.

	ON			OFF		
	Total	Percentage of recordings	Number of hemispheres	Total	Percentage of recordings	Number of hemispheres
Theta/alpha only	16	13.33%	10	5	5.95%	3
Beta only	40	33.33%	20	40	47.62%	20
Both peaks	34	28.33%	19	14	16.67%	10
No peaks	30	25.00%	15	25	29.76%	13

pairs as (i) only containing a coherence peak in the theta/alpha range; (ii) only containing a peak in the beta range; (iii) containing peaks in both theta/alpha and beta ranges; or (iv) without any discernible peaks (Fig. 3A). The number of assigned contact pairs in each category are summarized in Table 1. Coherence peaks in the theta/alpha range were more often detected in ON medication compared to OFF medication recordings, therefore making the comparison of theta/alpha and beta peak locations from ON medication recordings more reliable. A visualization of the electrode locations from which ON recordings in each category were taken revealed most recordings with theta/alpha coherence peaks only to be located ventrally near the border (as inferred from a winner-takes-all mapping of structural cortico-STN connections) of sensorimotor and cognitive/associative subregions, while beta peak locations were found in more dorsal locations and across a larger volume of the sampled space (Fig. 3B, see also Supplementary Fig. 2 for a visualization in the standard anatomical planes). Nevertheless, theta/alpha peaks were also detected in large parts of the dorsolateral STN but mostly together with the presence of a beta peak. For OFF recordings, the trend of theta/alpha coherence to occur towards the sensorimotor and cognitive/associative border was mostly visible in the locations of recordings with both theta/alpha and beta coherence peaks. The few locations with only theta/alpha peaks were situated either at the sensorimotor and cognitive/associative border or more posterior, inside the sensorimotor region or outside the STN. Notably, electrode locations for which no discernible coherence peaks were observed were found both within and outside the STN.

The mean MNI coordinates of the electrode locations in each category are summarized in Table 2. A systematic comparison revealed that for ON recordings, locations with theta/alpha peaks only and with both peaks were situated significantly inferior (lower z-coordinates) compared to beta peaks only (resp. $t(54) = -2.70$, $p = .009$; $t(72) = -2.82$, $p = .006$). Locations with both peaks were situated significantly more posterior (lower y-coordinates) compared to theta/alpha peaks only and beta peaks only (resp. $t(48) = -2.50$, $p = .016$; $t(72) = -3.58$, $p = .001$). For OFF recordings, theta/alpha peaks only were situated more posterior compared to beta peaks only ($t(43) = -2.06$, $p = .045$) but this finding should be carefully interpreted due to the low number of available data points. Only a trend was observed for locations without identified peaks to differ in x-coordinates compared to locations with identified peaks (ON: $t(118) = 1.69$, $p = .094$; OFF: $t(82) = -1.98$, $p = .051$). The coor-

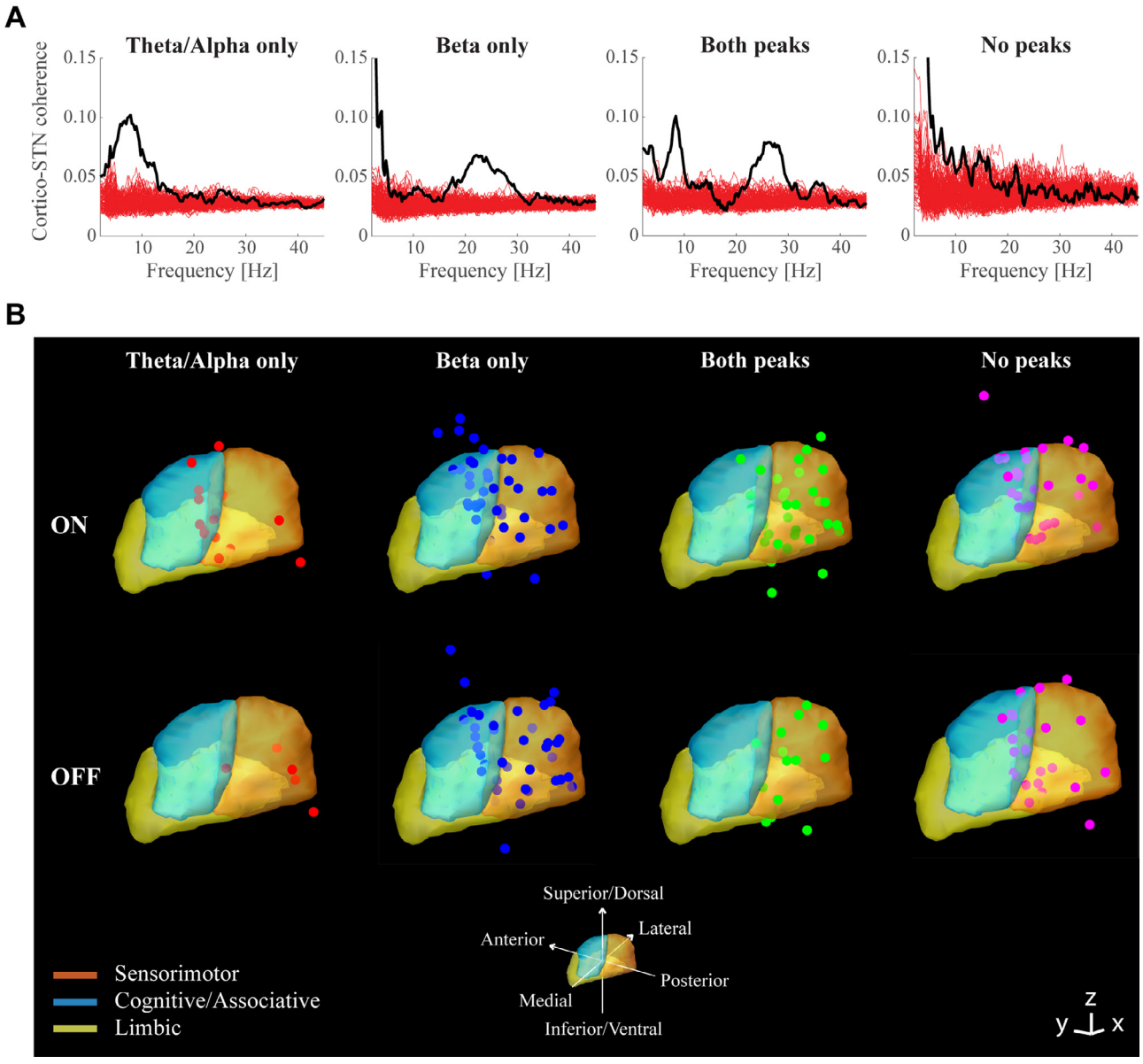

Fig. 3. Classification of recordings based on the presence of peaks in the cortico-STN coherence spectrum. (A) Example coherence spectra for each of the four categories. Black lines represent the observed spectrum for one of the STN contact pairs with coherence values averaged over all MEG sensors. Red lines indicate the 100 spectra obtained after shuffling the order of epochs for the STN data. (B) Visualization of recording sites within each category. Each dot represents the Euclidean midpoint between the two electrode contacts from which the bipolar derivation was taken. Recordings ON medication are shown in the top row, recordings OFF medication in the bottom row. The STN is visualized according to the Distal atlas (Ewert et al., 2018) with its subregions as derived from human tractography data. All data points were projected and visualized onto the STN in the right hemisphere.

Table 2
Average coordinates for identified locations in each coherence category.

	MNI			MCP		
	X	Y	Z	X	Y	Z
ON						
Theta/alpha only	11.38 (±0.98)	−13.63 (±1.91)	−7.34 (±1.86)	11.70 (±0.90)	−1.65 (±1.70)	−3.48 (±1.62)
Beta only	11.65 (±0.74)	−13.34 (±2.16)	−5.74 (±2.05)	12.04 (±0.91)	−1.58 (±2.24)	−2.09 (±1.82)
Both peaks	11.81 (±1.10)	−14.98 (±1.71)	−7.10 (±2.08)	10.93 (±2.55)	−2.86 (±1.93)	−3.11 (±1.71)
No peaks	12.00 (±0.98)	−13.47 (±1.83)	−5.88 (±2.03)	12.33 (±0.98)	−1.62 (±1.81)	−2.15 (±1.75)
OFF						
Theta/alpha only	12.49 (±1.49)	−16.35 (±1.96)	−7.66 (±1.46)	12.16 (±1.36)	−3.78 (±1.99)	−3.71 (±1.41)
Beta only	11.85 (±0.96)	−14.18 (±2.25)	−6.00 (±2.25)	11.61 (±2.23)	−1.94 (±2.31)	−2.25 (±1.81)
Both peaks	11.61 (±1.08)	−14.98 (±1.33)	−6.80 (±2.32)	12.00 (±2.39)	−3.37 (±2.11)	−3.18 (±1.80)
No peaks	11.38 (±0.84)	−14.10 (±1.82)	−6.77 (±2.00)	11.58 (±0.88)	−2.24 (±1.72)	−2.74 (±1.78)

Standard deviations are indicated in brackets. For reference purposes, AC/PC coordinates relative to the midcommissural point (MCP) were computed using the conversion tool by (Horn et al., 2017a). All coordinates are expressed in mm.

dinates of locations with and without peaks did not differ in the other dimensions.

These comparisons were repeated after projecting all data points onto the three principal axes of the STN in order to interpret the relative locations with respect to the dimensions of the STN. For ON recordings, this revealed that theta/alpha peaks only were situated more ventromedial along the longitudinal axis of the STN compared to locations with both peaks ($t(48) = 2.36$, $p = .022$). A similar trend was observed for beta peaks only compared to both peaks ($t(72) = 1.73$, $p = .088$). The second principal axis intersects the ventral and dorsal borders of the STN. Here, beta peaks only were found at significantly superior locations compared to both peaks ($t(72) = 3.89$, $p < .001$) ON medication, and to theta/alpha peaks only OFF medication ($t(43)=2.17$, $p = .036$). A trend was observed between beta peaks and theta/alpha peaks only ON medication ($t(54)=1.99$, $p = .051$). Another trend was observed between beta peaks and theta/alpha peaks only along the third (left-right) principal axis of the STN ($t(54) = -1.86$, $p = .069$). Again, locations without identified peaks in ON recordings only showed a trend to be situated more superior compared to locations with identified peaks ($t(118) = 1.84$, $p = .068$), and more ventromedial along the longitudinal axis for OFF medication recordings ($t(82) = 1.90$, $p = .061$). Findings are summarized in Fig. 4A.

Finally, non-parametric tests were performed to determine whether locations within a category were more spatially clustered than expected by chance. The average Euclidean distance between each electrode location and the centre of the point cloud for each cluster was compared against the distribution of distances obtained with shuffled category labels. Although none of the observed distance values were found to be smaller than the 5th percentile of the control distribution, a trend was observed for theta/alpha peaks only in the ON condition ($p = .08$). For OFF medication, the lowest p-value was found for the both peaks category ($p = .12$). A selection of performed tests is visualized in Fig. 4B.

4. Discussion

We found evidence for regional specialization within the STN region based on the functional connectivity profile between LFP and MEG recordings. Two frequency-specific (sub-)cortico-STN networks could be identified in most participants: theta/alpha coherence with the thalamus and (Rolandic) operculum, and beta coherence with pre-motor cortex. Although these networks were found to be largely independent of medication state, distinct peaks in the coherence spectrum were more often identified in recordings obtained ON medication. The sites of LFP recordings with a coherence peak in the theta/alpha frequency range only were located significantly more inferior than recordings with only beta coherence peaks, and appeared predominantly around the border between cognitive/associative and sensorimotor subregions, as previously determined from the structural connectivity profile of the STN (Ewert et al., 2018). Nevertheless, recordings with beta coherence peaks were still observed in the same region, and recordings with both theta/alpha and beta coherence peaks appeared through much of the sensorimotor subregion. The large variability and overlap in spatial locations suggest that these functional networks might not be clearly segregable into spatially distinct parts of the STN or that the limited spatial resolution of macro-electrode recordings was not able to capture sharp borders.

Our findings expand on previous work outlining the spatial distribution of spectral power within the STN region. Geng et al. (2018) demonstrated that peak amplitude values in different frequency bands are spatially clustered despite similarly large interindividual variability as for our coherence peaks. Beta oscillations are frequently reported to be strongest in the dorsolateral part of the STN, at around 1–3 mm below the dorsal border (de Solages et al., 2011; Kühn et al., 2005b; Seifried et al., 2012; Trottenberg et al., 2007; Weinberger et al., 2006; Zaidel et al., 2010). Using a large data set, Horn et al. (2017b) found alpha band power to be highest at a similar part of the STN as our theta/alpha coherence cluster. Gamma band activity (60–90 Hz) and high-frequency oscillations (HFO) appear to be pronounced at sites around the STN's dorsal border, hence slightly superior to the beta band (Geng et al., 2018; Trottenberg et al., 2006; van Wijk et al., 2017b) but have also been reported more central in the dorsolateral part (Telkes et al., 2018; Wang et al., 2014; Zaidel et al., 2010).

The regional variation in the manifestation of spectral components suggests that different parts of the STN may contribute to different functions. Although stimulus-locked and response-locked time-frequency modulations have been observed during various cognitive and behavioural tasks e.g., Alegre et al. (2010), Anzak et al. (2011), Brittain et al. (2012), Herz et al. (2016), Kühn et al. (2006a), (2005a), Oswal et al. (2013b), Schroll et al. (2018), Tan et al. (2016), Zénon et al. (2016), the anatomical coordinates of electrode contacts with maximum signal change have not always been systematically investigated. Studies that did take the location of recordings into account present spatially diffuse movement-induced modulations in beta and gamma power that appear strongest in the dorsolateral part of the STN (Geng et al., 2018; Lofredi et al., 2018; Tinkhauser et al., 2019). Additionally, theta/alpha modulations associated with the processing of affective pictures have been found near the ventral border (Rappel et al., 2020). These observations are reminiscent of the scattered peak locations we found for cortico-STN beta coherence and the seemingly more confined alpha coherence cluster that was located more ventromedially, hence potentially linking local task-induced activations with long-range functional networks.

The cortical sources we identified for the presented theta/alpha and beta coherence are very similar to those reported by Litvak et al. (2011a) and Hirschmann et al. (2011) with independent data sets. Compared to Litvak et al. (2011a), the deep theta/alpha source was more pronounced. Given the low sensitivity of MEG to activity from subcortical structures, it is fair to question the validity of this identified source. It is possible that the presence of correlated activity from lateral cortical sources in the left and right hemispheres, as the sensor-level topographies for left STN might suggest, may have led to localization errors. Furthermore, MEG is limited in its ability to distinguish the contribution of individual structures at locations deep inside the brain, therefore leaving open the possibility that the coherence source assigned to the thalamus in the present study has its origin in the brainstem, as identified by Litvak et al. (2011a). The cortical source assigned to the Rolandic operculum emerged at nearly the same peak coherence value in the grand-average coherence images (top row Fig. 2), and is therefore likely to also contribute strongly to the sensor-level coherence spectra upon which all other analyses are based. For these reasons, we still prefer to refer to the identified networks as 'cortico-STN' coherence. Hirschmann et al. (2011) also investigated the distribution of alpha and beta cortico-STN coherence peaks across DBS electrode contact pairs. They observed alpha coherence to be homogeneously distributed across contact pairs, while beta coherence appeared more focal. By contrast, beta coherence peaks were often detected across multiple contact pairs per hemisphere in our study. Interestingly however, Hirschmann et al. (2011) report the lowest beta coherence values (although not significantly different) for the lowest contact pair of the electrode, which is in line with the more superior locations we observed for locations with beta coherence only.

Evidence for analogous networks in the same frequency ranges is starting to emerge for other subcortical structures as well, including the external pallidum (Neumann et al., 2015) and pedunculopontine nucleus (Jha et al., 2017). Hence, these functional connections do not seem to be specific for the STN but could be part of larger networks involving multiple structures. In line with the common association between beta oscillations and motor control, cortico-subcortical beta coherence is strongest with motor cortical areas, and decreases during movement (Hirschmann et al., 2013; Lalo et al., 2008; van Wijk et al., 2017a). The role of the cortico-subcortical alpha coherence network is presently less understood but weaker pallido-cerebellar coupling has been linked to

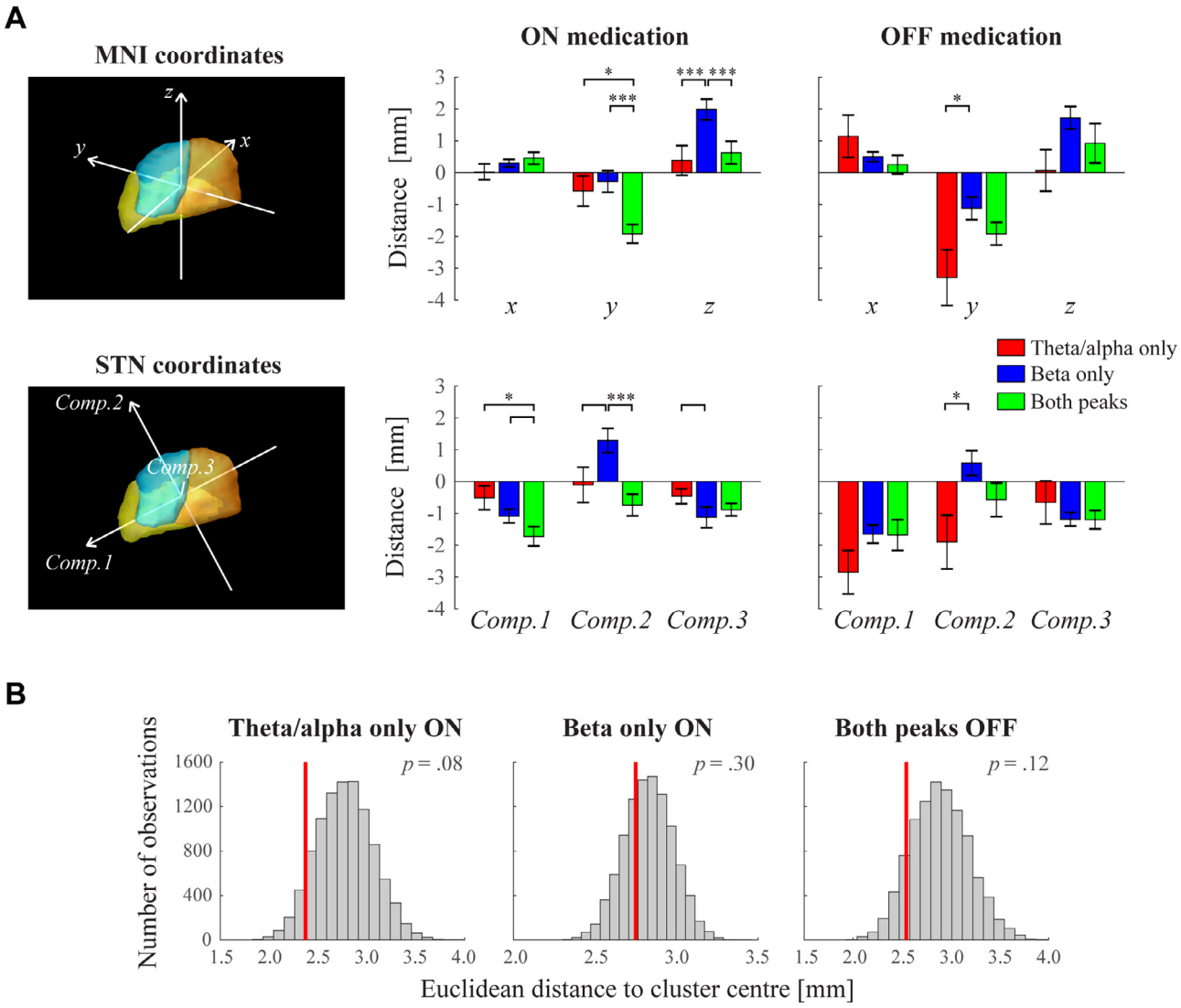

Fig. 4. Statistical evaluation of electrode locations with theta/alpha and beta coherence. (A) Pair-wise independent samples *t*-tests between coherence categories for each dimension of the MNI coordinate system (top row) and along the three principal axes of the STN (bottom row). Significant effects with $p < .05$ are indicated with *, effects with $p < .001$ are indicated with ***. Effects indicated without * signify *p*-values between .05 and .10. Error bars represent standard errors. For visualization purposes, the origin of both coordinate systems was chosen at the centre of the STN, corresponding to MNI coordinates $x = 11.35$, $y = -13.06$, $z = -7.73$. True MNI coordinates for each coherence category are reported in Table 1. (B) Non-parametric evaluation of the degree of spatial clustering. Red bars indicate the observed Euclidean distance between each point within the coherence category and the centre of the point cloud. The control distribution obtained after shuffling the category labels of contact pairs is depicted in grey. A selection of performed tests is shown.

higher symptom severity in dystonia patients (Neumann et al., 2015). Cortico-STN theta band coherence is less frequently reported for rest recordings but emerges with midfrontal cortical regions during conflict and response inhibition in decision-making tasks (Zavala et al., 2016, 2014), for which it appears strongest in recordings from ventral DBS electrodes (Alegre et al., 2013). It remains to be clarified whether this theta activation is specific to the STN as inhibitor of (premature) motor output or could also be detected in other subcortical structures. Nonetheless, task-related LFP recordings from DBS electrodes make it increasingly clear that subcortical structures like the STN are involved in many behaviourally-relevant aspects that may be processed via (partially) separated cortico-subcortical circuits.

Despite the clear effect of dopaminergic medication on the alleviation of motor symptoms in people with Parkinson's disease, no systematic effects of levodopa on cortico-STN coherence have been found across studies. While Litvak et al. (2011a) found beta band coherence to be increased with medication for a small number of voxels in prefrontal cortex, others report decreased values (Hirschmann et al., 2013) or no significant change (Lalo et al., 2008). In the present study, sensor-level coherence was found to be higher for OFF recordings in frequency bins that did not coincide with peak frequencies identified in individual spectra. In fact, distinct peaks in individual coherence spectra were less frequently observed in OFF compared to ON recordings. Interestingly, Rodriguez-Oroz et al. (2011) reported that levodopa administration could induce a spectral peak in the theta/alpha frequency range of STN-LFP recordings in patients who experienced medication-related side effects. This peak was located at more ventral recording sites for patients who were diagnosed with behavioural side effects in the form of impulse control disorders compared to patients with motor side effects in the form of dystonia. Both groups also showed elevated theta/alpha cortico-STN coherence compared to patients without side effects. Although the subjects in our study did not present with clinically significant side effects during the recordings, we did observe that the intake of medication led to more prominent coherence peaks in the theta/alpha

range. While we also explored the spatial distribution of average coherence values in the theta/alpha and beta ranges, no evidence for regional specialization was observed. A similar lack of evidence was found for the distribution of peak coherence values, suggesting that considering the presence of coherence peaks as binary information might eliminate some of the random variance due to interindividual differences in raw coherence values. Nonetheless, the low number of theta/alpha peaks in OFF recordings complicates a direct comparison of spatial distributions in the STN between medication states.

Findings of this study should be interpreted with a few methodological limitations in mind. First of all, we were unable to map coherence peaks across the entire volume of the STN due to unequal spatial sampling. As expected, most electrodes were implanted close to the surgical target in the dorsolateral part of the STN, hence no recordings were available from the ventromedial tip. Judging from the location of theta/alpha coherence peaks, it is conceivable that the cluster of peak locations further extends into the putative cognitive/associative and possibly limbic subregions. Sampling only the most dorsolateral part of the distribution of theta/alpha peaks may have resulted in lower evidence for spatial clustering, for which we only found a statistical trend.

Secondly, the limited spatial resolution of LFP recordings might have contributed to the relatively large spatial overlap between theta/alpha and beta coherence. Identified locations are the Euclidean midpoint between the two electrode contacts used in the bipolar derivation for obtaining the STN time series. Each contact is sensitive to neural activity within a volume that may extend up to several millimetre (Lempka and McIntyre, 2013). It is therefore possible that some time series reflect activity from surrounding structures like the thalamus (located superior to the STN) or substantia nigra (located inferior to the STN), or that contacts localized outside the STN still pick up activity that is generated within the nucleus. Hence, we adopt the term 'STN region' in his manuscript. However, theta/alpha and beta band coherence are likely to be equally affected by the limited spatial resolution, therefore their relative locations are still expected to be informative.

Thirdly, as discussed in Horn et al. (2019), inaccuracies in the localization of DBS electrodes may arise at different stages of the processing pipeline including the electrode reconstruction step and the warping of individual scans to MNI space. While it is difficult to quantify these inaccuracies, previous studies have verified the correspondence between the centre of the electrode and the observed artifact in MRI and CT using phantom experiments (Hemm et al., 2009; Husch et al., 2017; Yelnik et al., 2003). In addition, a comparative study of nonlinear registration algorithms showed that the applied ANTs SyN method (with the multispectral default preset implemented in Lead-DBS) resulted in more accurate segmentations of the STN than most other automatic algorithms and its performance was comparable to that of expert manual raters (Ewert et al., 2019). The warping to MNI space was necessary in order to create a spatial distribution of coherence locations across patients and hemispheres, to facilitate statistical analyses on the group-level, and to make use of the previously developed DISTAL atlas for visualization of STN subregions (based on diffusion-weighted MRI). We point out that outlining the poorly visible STN borders on individual patient scans in native space arguably would have led to localization errors as well. It should be noted that not all contact location centers that reside outside the STN in our visualizations are due to localization errors. Given the relatively wide 2 mm contact spacing of the electrode model and imprecisions that might arise during the surgical procedure, a substantial proportion of contact centers can be expected to be truly located outside the STN.

Finally, the selection of coherence peaks and their visual inspection is prone to arbitrary decisions. Overall, we took a conservative approach by only selecting a peak when it clearly stood out from the background. For some recordings this was more difficult to determine in the lower frequency range of the coherence spectrum, which could be the reason for the lower number of peaks selected for the theta/alpha range compared to the beta band. As a consequence, we might have underestimated the true number of theta/alpha and beta peaks, which could have contributed to the relatively large number of electrode locations within the STN that were categorized as having no discernible peaks.

Understanding the structural and functional organisation of the STN and its embedment within brain-wide networks is crucial for optimizing DBS treatment (van Wijk et al., 2020). Although the dorsolateral (sensorimotor) part of the STN is often chosen as surgical target for implanting DBS electrodes for treatment of Parkinson's disease, some studies report even better clinical outcomes for active electrodes located above the STN's superior border (Plaha et al., 2006; Voges et al., 2002), hence outside the nucleus. Which distant brain regions are likely to be influenced by the stimulation of fibre tracts can be estimated by combining diffusion-weighted imaging with computer simulations of the volume of activated tissue. In this way, specific (f)MRI connectivity profiles can be identified that are associated with a reduction of motor symptoms when stimulated (Horn et al., 2017c). It remains to be established whether theta/alpha and beta cortico-STN networks are similarly predictive for treatment outcome. Of note is that the average MNI coordinates of identified locations with only beta coherence peaks in the present study are closer to the location of DBS contacts commonly used for chronic stimulation ([x=12.58 y=−13.41 z=−5.87] as determined by meta-analysis of 8 studies from multiple centres (Caire et al., 2013; Horn et al., 2017a)), than the average MNI coordinates for locations with theta/alpha coherence peaks only and both peaks. So far, however, DBS has been found to suppress beta coherence with mesial premotor regions but not in a systematic way compared to observed motor improvement (Oswal et al., 2016).

DBS treatment frequently results in neuropsychiatric side effects related to cognition and affective behaviour in addition to an alleviation of motor symptoms (Benabid et al., 2009; Voon et al., 2006). The large degree of overlap in locations with theta/alpha and beta coherence peaks suggests that functional networks related to cognitive and motor functions might not be clearly spatially segregable (van Wijk et al., 2020). Likewise, the distinction between separate theta, alpha, and beta frequency bands is not always clear-cut (Accolla et al., 2017), also not when correlating spectral power with clinical symptoms (Kühn et al., 2006b; Neumann et al., 2016). It could be very challenging to fully prevent adverse effects of stimulation when neural representations are highly intermingled or shared between modalities. On the other hand, technological advances such as current steering (Contarino et al., 2014) and closed-loop applications (Little et al., 2013) will give clinicians a more flexible control over stimulation settings. The present work may contribute towards a more detailed understanding of which structural and functional cortico-basal ganglia networks should be targeted with DBS, and towards the detection of potential electrophysiological biomarkers for adaptive stimulation.

Data and code availability statements

The open source Matlab toolboxes that were used in this study can be obtained from:

Lead-DBS: https://www.lead-dbs.org

SPM12: http://www.fil.ion.ucl.ac.uk/spm

Fieldtrip: http://fieldtriptoolbox.org

Custom-written Matlab scripts are available for sharing upon request. Local ethics and clinical privacy issues prohibit sharing of individual imaging data.

Funding

This research was supported by the European Union's Horizon 2020 research and innovation programme under the Marie Sklodowska-Curie grant agreement No 795866 (B.C.M.v.W.), W.J.N., A.H., and A.A.K. received funding from the Deutsche Forschungsgemeinschaft (DFG (German Research Foundation) – Project-ID 424778381 – TRR 295; A.H. received also Grant 410169619), D.K. was supported by the

BIH-Charité Clinician Scientist Program funded by the Charité - Universitätsmedizin Berlin and the Berlin Institute of Health, A.H. was supported by the National Institutes of Health (2R01 MH113929) as well as the New Venture Fund (FFOR Seed Grant), T.S. relied on the DFG Core Facility "Metrology of Ultra-Low Magnetic Fields" grant number KO5321/3 and TR408/11. The Wellcome Centre for Human Neuroimaging is supported by core funding from Wellcome (203147/Z/16/Z). This is an EU Joint Programme - Neurodegenerative Disease (JPND) project. The project is supported through the following funding organisations under the aegis of JPND - www.jpnd.eu (B.C.M.v.W.: the Netherlands Organisation for Health Research and Development (ZonMw) - The Netherlands; A.H.: the Deutsches Zentrum für Luft- und Raumfahrt - Germany).

Credit authorship contribution statement

Bernadette C.M. van Wijk: Conceptualization, Formal analysis, Writing – original draft. **Wolf-Julian Neumann:** Writing – review & editing. **Daniel Kroneberg:** Writing – review & editing. **Andreas Horn:** Software, Writing – review & editing. **Friederike Irmen:** Data curation, Writing – review & editing. **Tilmann H. Sander:** Writing – review & editing. **Qiang Wang:** Writing – review & editing. **Vladimir Litvak:** Software, Writing – review & editing. **Andrea A. Kühn:** Funding acquisition, Conceptualization, Writing – review & editing.

Supplementary materials

Supplementary material associated with this article can be found, in the online version, at doi:10.1016/j.neuroimage.2022.119320.

References

Accolla, E.A., Dukart, J., Helms, G., Weiskopf, N., Kherif, F., Lutti, A., Chowdhury, R., Hetzer, S., Haynes, J.D., Kühn, A.A., Draganski, B., 2014. Brain tissue properties differentiate between motor and limbic basal ganglia circuits. Hum. Brain Mapp. 35, 5083–5092. doi:10.1002/hbm.22533.

Accolla, E.A., Horn, A., Herrojo-Ruiz, M., Neumann, W.J., Kühn, A.A., 2017. Reply: oscillatory coupling of the subthalamic nucleus in obsessive compulsive disorder. Brain 140. doi:10.1093/BRAIN/AWX165.

Alegre, M., Lopez-Azcarate, J., Obeso, I., Wilkinson, L., Rodriguez-Oroz, M.C., Valencia, M., Garcia-Garcia, D., Guridi, J., Artieda, J., Jahanshahi, M., Obeso, J.A., 2013. The subthalamic nucleus is involved in successful inhibition in the stop-signal task: a local field potential study in Parkinson's disease. Exp. Neurol. 239, 1–12. doi:10.1016/j.expneurol.2012.08.027.

Alegre, M., Rodríguez-Oroz, M.C., Valencia, M., Pérez-Alcázar, M., Guridi, J., Iriarte, J., Obeso, J.A., Artieda, J., 2010. Changes in subthalamic activity during movement observation in Parkinson's disease: is the mirror system mirrored in the basal ganglia? Clin. Neurophysiol. 121, 414–425. doi:10.1016/j.clinph.2009.11.013.

Alkemade, A., Schnitzler, A., Forstmann, B.U., 2015. Topographic organization of the human and non-human primate subthalamic nucleus. Brain Struct. Funct. 220, 3075–3086. doi:10.1007/s00429-015-1047-2.

Anzak, A., Gaynor, L., Beigi, M., Limousin, P., Hariz, M., Zrinzo, L., Foltynie, T., Brown, P., Jahanshahi, M., 2011. A gamma band specific role of the subthalamic nucleus in switching during verbal fluency tasks in Parkinson's disease. Exp. Neurol. 232, 136–142. doi:10.1016/j.expneurol.2011.07.010.

Avants, B.B., Epstein, C.L., Grossman, M., Gee, J.C., 2008. Symmetric diffeomorphic image registration with cross-correlation: evaluating automated labeling of elderly and neurodegenerative brain. Med. Image Anal. 12, 26–41. doi:10.1016/J.MEDIA.2007.06.004.

Benabid, A.L., Chabardes, S., Mitrofanis, J., Pollak, P., 2009. Deep brain stimulation of the subthalamic nucleus for the treatment of Parkinson's disease. Lancet Neurol. 8, 67–81. doi:10.1016/S1474-4422(08)70291-6.

Brittain, J.S., Watkins, K.E., Joundi, R.A., Ray, N.J., Holland, P., Green, A.L., Aziz, T.Z., Jenkinson, N., 2012. A role for the subthalamic nucleus in response inhibition during conflict. J. Neurosci. 32, 13396–13401. doi:10.1523/JNEUROSCI.2259-12.2012.

Caire, F., Ranoux, D., Guehl, D., Burbaud, P., Cuny, E., 2013. A systematic review of studies on anatomical position of electrode contacts used for chronic subthalamic stimulation in Parkinson's disease. Acta Neurochir. 155, 1647–1654. doi:10.1007/s00701-013-1782-1.

Contarino, M.F., Bour, L.J., Verhagen, R., Lourens, M.A.J., de Bie, R.M.A., van den Munckhof, P., Schuurman, P.R., 2014. Directional steering: a novel approach to deep brain stimulation. Neurology 83, 1163–1169. doi:10.1212/WNL.0000000000000823.

de Solages, C., Hill, B.C., Yu, H., Henderson, J.M., Bronte-Stewart, H., 2011. Maximal subthalamic beta hypersynchrony of the local field potential in Parkinson's disease is located in the central region of the nucleus. J. Neurol. Neurosurg. Psychiatry 82, 1387–1389. doi:10.1136/jnnp.2010.223107.

Ewert, S., Horn, A., Finkel, F., Li, N., Kühn, A.A., Herrington, T.M., 2019. Optimization and comparative evaluation of nonlinear deformation algorithms for atlas-based segmentation of DBS target nuclei. Neuroimage 184, 586–598. doi:10.1016/j.neuroimage.2018.09.061.

Ewert, S., Plettig, P., Li, N., Chakravarty, M.M., Collins, D.L., Herrington, T.M., Kühn, A.A., Horn, A., 2018. Toward defining deep brain stimulation targets in MNI space: a subcortical atlas based on multimodal MRI, histology and structural connectivity. Neuroimage 170, 271–282. doi:10.1016/j.neuroimage.2017.05.015.

Fonov, V., Evans, A.C., Botteron, K., Almli, C.R., McKinstry, R.C., Collins, D.L., 2011. Unbiased average age-appropriate atlases for pediatric studies. Neuroimage 54, 313–327. doi:10.1016/J.NEUROIMAGE.2010.07.033.

Geng, X., Xu, X., Horn, A., Li, N., Ling, Z., Brown, P., Wang, S., 2018. Intra-operative characterisation of subthalamic oscillations in Parkinson's disease. Clin. Neurophysiol. 129, 1001–1010. doi:10.1016/j.clinph.2018.01.075.

Gross, J., Kujala, J., Hamalainen, M., Timmermann, L., Schnitzler, A., Salmelin, R., 2001. Dynamic imaging of coherent sources: studying neural interactions in the human brain. Proc. Natl. Acad. Sci. U. S. A. 98, 694–699. doi:10.1073/pnas.98.2.694.

Haynes, W.I.A., Haber, S.N., 2013. The organization of prefrontal-subthalamic inputs in primates provides an anatomical substrate for both functional specificity and integration: implications for Basal Ganglia models and deep brain stimulation. J. Neurosci. 33, 4804–4814. doi:10.1523/JNEUROSCI.4674-12.2013.

Hemm, S., Coste, J., Gabrillargues, J., Ouchchane, L., Sarry, L., Caire, F., Vassal, F., Nuti, C., Derost, P., Durif, F., Lemaire, J.J., 2009. Contact position analysis of deep brain stimulation electrodes on post-operative CT images. Acta Neurochir. 151, 823–829. doi:10.1007/S00701-009-0393-3.

Herz, D.M., Zavala, B.A., Bogacz, R., Brown, P., 2016. Neural correlates of decision thresholds in the human subthalamic nucleus. Curr. Biol. 26, 916–920. doi:10.1016/j.cub.2016.01.051.

Hirschmann, J., Özkurt, T.E., Butz, M., Homburger, M., Elben, S., Hartmann, C.J., Vesper, J., Wojtecki, L., Schnitzler, A., 2013. Differential modulation of STN-cortical and cortico-muscular coherence by movement and levodopa in Parkinson's disease. Neuroimage 68, 203–213. doi:10.1016/j.neuroimage.2012.11.036.

Hirschmann, J., Özkurt, T.E., Butz, M., Homburger, M., Elben, S., Hartmann, C.J., Vesper, J., Wojtecki, L., Schnitzler, A., 2011. Distinct oscillatory STN-cortical loops revealed by simultaneous MEG and local field potential recordings in patients with Parkinson's disease. Neuroimage 55, 1159–1168. doi:10.1016/j.neuroimage.2010.11.063.

Horn, A., Kühn, A.A., 2015. Lead-DBS: a toolbox for deep brain stimulation electrode localizations and visualizations. Neuroimage 107, 127–135. doi:10.1016/j.neuroimage.2014.12.002.

Horn, A., Kühn, A.A., Merkl, A., Shih, L., Alterman, R., Fox, M., 2017a. Probabilistic conversion of neurosurgical DBS electrode coordinates into MNI space. Neuroimage 150, 395–404. doi:10.1016/j.neuroimage.2017.02.004.

Horn, A., Li, N., Dembek, T.A., Kappel, A., Boulay, C., Ewert, S., Tietze, A., Husch, A., Perera, T., Neumann, W.J., Reisert, M., Si, H., Oostenveld, R., Rorden, C., Yeh, F.C., Fang, Q., Herrington, T.M., Vorwerk, J., Kühn, A.A., 2019. Lead-DBS v2: towards a comprehensive pipeline for deep brain stimulation imaging. Neuroimage 184, 293–316. doi:10.1016/j.neuroimage.2018.08.068.

Horn, A., Neumann, W.J., Degen, K., Schneider, G.H., Kühn, A.A., 2017b. Toward an electrophysiological "sweet spot" for deep brain stimulation in the subthalamic nucleus. Hum. Brain Mapp. 38, 3377–3390. doi:10.1002/hbm.23594.

Horn, A., Reich, M., Vorwerk, J., Li, N., Wenzel, G., Fang, Q., Schmitz-Hübsch, T., Nickl, R., Kupsch, A., Volkmann, J., Kühn, A.A., Fox, M.D., 2017c. Connectivity predicts deep brain stimulation outcome in Parkinson's disease. Ann. Neurol. 82, 67–78. doi:10.1002/ana.24974.

Husch, A.V., Petersen, M., Gemmar, P., Goncalves, J., Hertel, F., 2017. PaCER - a fully automated method for electrode trajectory and contact reconstruction in deep brain stimulation. NeuroImage Clin. 17, 80–89. doi:10.1016/J.NICL.2017.10.004.

Jha, A., Litvak, V., Taulu, S., Thevathasan, W., Hyam, J.A., Foltynie, T., Limousin, P., Bogdanovic, M., Zrinzo, L., Green, A.L., Aziz, T.Z., Friston, K., Brown, P., 2017. Functional connectivity of the pedunculopontine nucleus and surrounding region in Parkinson's disease. Cereb. Cortex 27, 54–67. doi:10.1093/cercor/bhw340.

Keuken, M.C., Uylings, H.B.M., Geyer, S., Schäfer, A., Turner, R., Forstmann, B.U., 2012. Are there three subdivisions in the primate subthalamic nucleus? Front. Neuroanat. 6, 14. doi:10.3389/fnana.2012.00014.

Kühn, A.A., Doyle, L., Pogosyan, A., Yarrow, K., Kupsch, A., Schneider, G.H.H., Hariz, M.I., Trottenberg, T., Brown, P., 2006a. Modulation of beta oscillations in the subthalamic area during motor imagery in Parkinson's disease. Brain 129, 695–706. doi:10.1093/brain/awh715.

Kühn, A.A., Hariz, M.I., Silberstein, P., Tisch, S., Kupsch, A., Schneider, G.H., Limousin-Dowsey, P., Yarrow, K., Brown, P., 2005a. Activation of the subthalamic region during emotional processing in Parkinson disease. Neurology 65, 707–713. doi:10.1212/01.wnl.0000174438.78399.bc.

Kühn, A.A., Kupsch, A., Schneider, G.H., Brown, P., 2006b. Reduction in subthalamic 8–35 Hz oscillatory activity correlates with clinical improvement in Parkinson's disease. Eur. J. Neurosci. 23, 1956–1960. doi:10.1111/j.1460-9568.2006.04717.x.

Kühn, A.A., Trottenberg, T., Kivi, A., Kupsch, A., Schneider, G.H., Brown, P., 2005b. The relationship between local field potential and neuronal discharge in the subthalamic nucleus of patients with Parkinson's disease. Exp. Neurol. 194, 212–220. doi:10.1016/j.expneurol.2005.02.010.

Lalo, E., Thobois, S., Sharott, A., Polo, G., Mertens, P., Pogosyan, A., Brown, P., 2008. Patterns of bidirectional communication between cortex and basal ganglia during movement in patients with Parkinson disease. J. Neurosci. 28, 3008–3016. doi:10.1523/JNEUROSCI.5295-07.2008.

Lambert, C., Zrinzo, L., Nagy, Z., Lutti, A., Hariz, M., Foltynie, T., Draganski, B., Ashburner, J., Frackowiak, R., 2012. Confirmation of functional zones within the human subthalamic nucleus: patterns of connectivity and sub-parcellation using diffusion weighted imaging. Neuroimage 60, 83–94. doi:10.1016/j.neuroimage.2011.11.082.

Lempka, S.F., McIntyre, C.C., 2013. Theoretical analysis of the local field potential in deep brain stimulation applications. PLoS One 8, e59839. doi:10.1371/journal.pone.0059839.

Little, S., Pogosyan, A., Neal, S., Zavala, B., Zrinzo, L., Hariz, M., Foltynie, T., Limousin, P., Ashkan, K., FitzGerald, J., Green, A.L., Aziz, T.Z., Brown, P., 2013. Adaptive deep brain stimulation in advanced Parkinson disease. Ann. Neurol. 74, 449–457. doi:10.1002/ana.23951.

Litvak, V., Eusebio, A., Jha, A., Oostenveld, R., Barnes, G., Foltynie, T., Limousin, P., Zrinzo, L., Hariz, M.I., Friston, K., Brown, P., 2012. Movement-related changes in local and long-range synchronization in Parkinson's disease revealed by simultaneous magnetoencephalography and intracranial recordings. J. Neurosci. 32, 10541–10553. doi:10.1523/JNEUROSCI.0767-12.2012.

Litvak, V., Jha, A., Eusebio, A., Oostenveld, R., Foltynie, T., Limousin, P., Zrinzo, L., Hariz, M.I., Friston, K., Brown, P., 2011a. Resting oscillatory cortico-subthalamic connectivity in patients with Parkinson's disease. Brain 134, 359–374. doi:10.1093/brain/awq332.

Litvak, V., Mattout, J., Kiebel, S., Phillips, C., Henson, R., Kilner, J., Barnes, G., Oostenveld, R., Daunizeau, J., Flandin, G., Penny, W., Friston, K., 2011b. EEG and MEG data analysis in SPM8. Comput. Intell. Neurosci. 2011, 1–32. doi:10.1155/2011/852961.

Lofredi, R., Neumann, W.J., Bock, A., Horn, A., Huebl, J., Siegert, S., Schneider, G.H., Krauss, J.K., Kühn, A.A., 2018. Dopamine-dependent scaling of subthalamic gamma bursts with movement velocity in patients with Parkinson's disease. Elife 7, e31895. doi:10.7554/eLife.31895.

Mattout, J., Henson, R.N., Friston, K.J., 2007. Canonical source reconstruction for MEG. Comput. Intell. Neurosci. 2007, 67613. doi:10.1155/2007/67613.

Nambu, A., Tokuno, H., Takada, M., 2002. Functional significance of the cortico-subthalamo-pallidal "hyperdirect" pathway. Neurosci. Res. 43, 111–117. doi:10.1016/S0168-0102(02)00027-5.

Neumann, W.J., Degen, K., Schneider, G.H., Brücke, C., Huebl, J., Brown, P., Kühn, A.A., 2016. Subthalamic synchronized oscillatory activity correlates with motor impairment in patients with Parkinson's disease. Mov. Disord. 31, 1748–1751. doi:10.1002/mds.26759.

Neumann, W.J., Jha, A., Bock, A., Huebl, J., Horn, A., Schneider, G., Sander, T.H., Litvak, V., Kühn, A.A., 2015. Cortico-pallidal oscillatory connectivity in patients with dystonia. Brain 138, 1894–1906. doi:10.1093/brain/awv109.

Nolte, G., 2003. The magnetic lead field theorem in the quasi-static approximation and its use for magnetoencephalography forward calculation in realistic volume conductors. Phys. Med. Biol. 48, 3637–3652. doi:10.1088/0031-9155/48/22/002.

Oostenveld, R., Fries, P., Maris, E., Schoffelen, J.M., 2011. FieldTrip: open source software for advanced analysis of MEG, EEG, and invasive electrophysiological data. Comput. Intell. Neurosci. 2011, 1–9. doi:10.1155/2011/156869.

Oswal, A., Beudel, M., Zrinzo, L., Limousin, P., Hariz, M., Foltynie, T., Litvak, V., Brown, P., 2016. Deep brain stimulation modulates synchrony within spatially and spectrally distinct resting state networks in Parkinson's disease. Brain 139, 1482–1496. doi:10.1093/brain/aww048.

Oswal, A., Brown, P., Litvak, V., 2013a. Movement related dynamics of subthalmocortical alpha connectivity in Parkinson's disease. Neuroimage 70, 132–142. doi:10.1016/j.neuroimage.2012.12.041.

Oswal, A., Litvak, V., Brücke, C., Huebl, J., Schneider, G., Kühn, A.A., Brown, P., 2013b. Cognitive factors modulate activity within the human subthalamic nucleus during voluntary movement in Parkinson's disease. J. Neurosci. 33, 15815–15826. doi:10.1523/JNEUROSCI.1790-13.2013.

Parent, A., Hazrati, L.N., 1995. Functional anatomy of the basal ganglia. II. The place of subthalamic nucleus and external pallidium in basal ganglia circuitry. Brain Res. Rev. 20, 128–154. doi:10.1016/0165-0173(94)00008-D.

Plaha, P., Ben-Shlomo, Y., Patel, N.K., Gill, S.S., 2006. Stimulation of the caudal zona incerta is superior to stimulation of the subthalamic nucleus in improving contralateral parkinsonism. Brain 129, 1732–1747. doi:10.1093/brain/awl127.

Rappel, P., Grosberg, S., Arkadir, D., Linetsky, E., Abu Snineh, M., Bick, A.S., Tamir, I., Valsky, D., Marmor, O., Abo Foul, Y., Peled, O., Gilad, M., Daudi, C., Ben-Naim, S., Bergman, H., Israel, Z., Eitan, R., 2020. Theta-alpha oscillations characterize emotional subregion in the human ventral subthalamic nucleus. Mov. Disord. 35, 337–343. doi:10.1002/mds.27910.

Rodriguez-Oroz, M.C., López-Azcárate, J., Garcia-Garcia, D., Alegre, M., Toledo, J., Valencia, M., Guridi, J., Artieda, J., Obeso, J.A., 2011. Involvement of the subthalamic nucleus in impulse control disorders associated with Parkinson's disease. Brain 134, 36–49. doi:10.1093/BRAIN/AWQ301.

Schroll, H., Horn, A., Runge, J., Lipp, A., Schneider, G.H., Krauss, J.K., Hamker, F.H., Kühn, A.A., 2018. Reinforcement magnitudes modulate subthalamic beta band activity in patients with Parkinson's disease. Sci. Rep. 8, 8621. doi:10.1038/s41598-018-26887-3.

Seifried, C., Weise, L., Hartmann, R., Gasser, T., Baudrexel, S., Szelényi, A., van de Loo, S., Steinmetz, H., Seifert, V., Roeper, J., Hilker, R., 2012. Intraoperative microelectrode recording for the delineation of subthalamic nucleus topography in Parkinson's disease. Brain Stimul. 5, 378–387. doi:10.1016/j.brs.2011.06.002.

Tan, H., Wade, C., Brown, P., 2016. Post-movement beta activity in sensorimotor cortex indexes confidence in the estimations from internal models. J. Neurosci. 36, 1516–1528. doi:10.1523/JNEUROSCI.3204-15.2016.

Telkes, I., Viswanathan, A., Jimenez-Shahed, J., Abosch, A., Ozturk, M., Gupte, A., Jankovic, J., Ince, N.F., 2018. Local field potentials of subthalamic nucleus contain electrophysiological footprints of motor subtypes of Parkinson's disease. Proc. Natl. Acad. Sci. U. S. A. 115, E8567–E8576. doi:10.1073/pnas.1810589115.

Temel, Y., Blokland, A., Steinbusch, H.W.M., Visser-Vandewalle, V., 2005. The functional role of the subthalamic nucleus in cognitive and limbic circuits. Prog. Neurobiol. 76, 393–413. doi:10.1016/j.pneurobio.2005.09.005.

Thomson, D.J., 1982. Spectrum estimation and harmonic analysis. Proc. IEEE 70, 1055–1096.

Tinkhauser, G., Shah, A.S., Fischer, P., Peterman, K., Debove, I., Nygyuen, K., Nowacki, A., Torrecillos, F., Khawaldeh, S., Tan, H., Pogosyan, A., Schuepbach, M., Pollo, C., Brown, P., 2019. Electrophysiological differences between upper and lower limb movements in the human subthalamic nucleus. Clin. Neurophysiol. 130, 727–738. doi:10.1016/j.clinph.2019.02.011.

Toledo, J.B., López-Azcárate, J., Garcia-Garcia, D., Guridi, J., Valencia, M., Artieda, J., Obeso, J., Alegre, M., Rodriguez-Oroz, M., 2014. High beta activity in the subthalamic nucleus and freezing of gait in Parkinson's disease. Neurobiol. Dis. 64, 60–65. doi:10.1016/j.nbd.2013.12.005.

Trottenberg, T., Fogelson, N., Kühn, A.A., Kivi, A., Kupsch, A., Schneider, G.H., Brown, P., 2006. Subthalamic gamma activity in patients with Parkinson's disease. Exp. Neurol. 200, 56–65. doi:10.1016/j.expneurol.2006.01.012.

Trottenberg, T., Kupsch, A., Schneider, G.H., Brown, P., Kühn, A.A., 2007. Frequency-dependent distribution of local field potential activity within the subthalamic nucleus in Parkinson's disease. Exp. Neurol. 205, 287–291. doi:10.1016/j.expneurol.2007.01.028.

van Wijk, B.C.M., Alkemade, A., Forstmann, B.U., 2020. Functional segregation and integration within the human subthalamic nucleus from a micro- and meso-level perspective. Cortex 131, 103–113. doi:10.1016/j.cortex.2020.07.004.

van Wijk, B.C.M., Neumann, W.J., Schneider, G.H., Sander, T.H., Litvak, V., Kühn, A.A., 2017a. Low-beta cortico-pallidal coherence decreases during movement and correlates with overall reaction time. Neuroimage 159, 1–8. doi:10.1016/j.neuroimage.2017.07.024.

van Wijk, B.C.M., Pogosyan, A., Hariz, M.I., Akram, H., Foltynie, T., Limousin, P., Horn, A., Ewert, S., Brown, P., Litvak, V., 2017b. Localization of beta and high-frequency oscillations within the subthalamic nucleus region. NeuroImage Clin. 16, 175–183. doi:10.1016/j.nicl.2017.07.018.

Voges, J., Volkmann, J., Allert, N., Lehrke, R., Koulousakis, A., Freund, H.J., Sturm, V., 2002. Bilateral high-frequency stimulation in the subthalamic nucleus for the treatment of Parkinson disease: correlation of therapeutic effect with anatomical electrode position. J. Neurosurg. 96, 269–279. doi:10.3171/jns.2002.96.2.0269.

Voon, V., Kubu, C., Krack, P., Houeto, J.L., Tröster, A.I., 2006. Deep brain stimulation: neuropsychological and neuropsychiatric issues. Mov. Disord. 21, S305–S327. doi:10.1002/mds.20963.

Wang, J., Hirschmann, J., Elben, S., Hartmann, C.J., Vesper, J., Wojtecki, L., Schnitzler, A., 2014. High-frequency oscillations in Parkinson's disease: spatial distribution and clinical relevance. Mov. Disord. 29, 1–8. doi:10.1002/mds.25962.

Weinberger, M., Mahant, N., Hutchison, W.D., Lozano, A.M., Moro, E., Hodaie, M., Lang, A.E., Dostrovsky, J.O., 2006. Beta oscillatory activity in the subthalamic nucleus and its relation to dopaminergic response in Parkinson's disease. J. Neurophysiol. 96, 3248–3256. doi:10.1152/jn.00697.2006.

Yelnik, J., Damier, P., Demeret, S., Gervais, D., Bardinet, E., Bejjani, B.P., François, C., Houeto, J.L., Arnulf, I., Dormont, D., Galanaud, D., Pidoux, B., Cornu, P., Agid, Y., 2003. Localization of stimulating electrodes in patients with Parkinson disease by using a three-dimensional atlas-magnetic resonance imaging coregistration method. J. Neurosurg. 99, 89–99. doi:10.3171/JNS.2003.99.1.0089.

Zaidel, A., Spivak, A., Grieb, B., Bergman, H., Israel, Z., 2010. Subthalamic span of β oscillations predicts deep brain stimulation efficacy for patients with Parkinson's disease. Brain 133, 2007–2021. doi:10.1093/brain/awq144.

Zavala, B., Tan, H., Ashkan, K., Foltynie, T., Limousin, P., Zrinzo, L., Zaghloul, K., Brown, P., 2016. Human subthalamic nucleus-medial frontal cortex theta phase coherence is involved in conflict and error related cortical monitoring. Neuroimage 137, 178–187. doi:10.1016/j.neuroimage.2016.05.031.

Zavala, B.A., Tan, H., Little, S., Ashkan, K., Hariz, M., Foltynie, T., Zrinzo, L., Zaghloul, K.A., Brown, P., 2014. Midline frontal cortex low-frequency activity drives subthalamic nucleus oscillations during conflict. J. Neurosci. 34, 7322–7333. doi:10.1523/JNEUROSCI.1169-14.2014.

Zénon, A., Duclos, Y., Carron, R., Witjas, T., Baunez, C., Régis, J., Azulay, J.P., Brown, P., Eusebio, A., 2016. The human subthalamic nucleus encodes the subjective value of reward and the cost of effort during decision-making. Brain 139, 1830–1843. doi:10.1093/brain/aww075.